

# Numerical analysis of a liquid metal cooled mini channel heat sink with five different ceramic substrates



Md Tanbir Sarowar

Department of Mechanical and Production Engineering, Islamic University of Technology, Board Bazar, 1704, Bangladesh

## ARTICLE INFO

### Keywords:

Engineering ceramics  
Numerical methods  
Liquid metal  
Microchannel heat sink

## ABSTRACT

Due to recent advancements in micro-electro-mechanical systems (MEMS), the requirements of extracting a huge heat flux from a small surface area is ever-increasing. The use of mini/microchannel heat sinks (MCHS) can contribute much to the cooling mechanisms of these MEMS. The improvements in mini/microchannel heat sinks are getting a lot of considerations recently for this reason. The improvements in the MCHS can be accelerated by the use of liquid metals as working fluids, as they possess excellent thermophysical properties. But using the liquid metals as coolants is still limited in the MCHS because of the possibilities of corrosions of the heat sink's substrate as it is often made of metals. The possible solution to this challenge can be using non-metallic materials (like ceramic materials) as the substrate material for the heat sinks, which possess resistive properties to corrosions and good heat transport properties as well. In this paper, the thermal performance of a mini channel heat sink with five different substrate materials (aluminum nitride, beryllium oxide, hafnium diboride, titanium diboride, and zirconium diboride) and four different alloys of gallium as working fluid (EGaInSn, EGaIn, GaIn and GaSn) are tested. The study also offers the effect of different geometry parameters of the rectangular channel on the overall performance of the heat sink. The thermal and hydraulic performance of the heat sink is analyzed by the 3D numerical model. The results are validated against data obtained from literature and theoretical correlations. It has been found that the heat sink made of aluminum nitride (AlN) shows superior performance than all other substrate materials. The optimum coolant material as found after the analysis is GaIn.

## 1. Introduction

Micro/mini channel heat sink is a miniaturized heat exchanger that can remove a huge amount of heat flux from a small surface area. The rapid developments in IT industries are also increasing huge challenges in the cooling mechanisms of the electronic components. As the sizes of the electronic devices are being reduced, the requirements of higher computing speed are also increasing rapidly. Their performance is greatly influenced by the cooling technologies associated with them. Keeping account of the challenges in the cooling techniques micro-channel heat sink was first formulated by Tuckerman and Pearse in the year 1981 [1]. They introduced a water-cooled silicon microchannel heat exchanger which could extract  $790\text{W}/\text{cm}^2$  of heat flux with the maximum increase in temperature of  $71^\circ\text{C}$ . Micro/mini channel heat sink can extract a huge heat flux from a small surface area due to the large forced convective heat transfer effects in the channels. But that also comes with the cost of large pressure drops in the channels which results in higher requirements of pumping powers. After pioneered by Tuckerman and Pearse in 1981, extensive works has been reported to

improve the thermal and hydraulic performances of the mini/micro channel heat sinks. The studies mainly focus on analytical [2,3], numerical [4–9], and experimental methods [10–13]. Various analytical models are used in evaluating the performance of these mini/micro heat exchangers like the porous medium model, the fin model, and the thermal resistance model [3].

Recently, the implementation of liquid metals with lower melting temperature is growing much interest in cooling technologies [14–17]. Though previously the applications of the liquid metal cooling technologies were limited to high-temperature applications because of the higher melting points of the liquid metals. To address this issue and increase the applications of liquid metal cooling technologies in other sectors several eutectic gallium alloys are prepared to lower the melting point of gallium liquid metal. Indium (In) was the first element that was alloyed with gallium to obtain EGaIn that could lower the melting point up to  $15^\circ\text{C}$  [18]. The next element was tin (Sn) which was combined with EGaIn to obtain EGaInSn, which could lower the melting point up to [19]. Both of these materials have been widely used in various cooling technologies especially in micro-electronics. Deng et al. [20]

E-mail address: [tanbirsarowar@iut-dhaka.edu](mailto:tanbirsarowar@iut-dhaka.edu).

<https://doi.org/10.1016/j.ceramint.2020.08.124>

Received 19 June 2020; Received in revised form 2 August 2020; Accepted 14 August 2020

Available online 20 August 2020

0272-8842/ © 2020 Elsevier Ltd and Techna Group S.r.l. All rights reserved.

compared the heat transfer coefficient obtained from GaIn<sub>20</sub> (Ga 80% and In 20%) and water in a microchannel heat sink experimentally. They showed that the heat sink having GaIn<sub>20</sub> can reach a superior heat transfer coefficient. Xiang et al. [21] compared liquid gallium with water by observing the total thermal resistance offered by the rectangular heat sink under similar conditions and showed that liquid gallium based heat sink can obtain a lower total thermal resistance than water. Yang et al. [22] showed Ga<sub>68</sub>In<sub>20</sub>Sn<sub>12</sub> exhibits much better flow and heat transfer properties than water. Despite having excellent thermophysical properties the use of these liquid metals in micro/mini channel heat sink is still rare due to the chances of corrosions or chemical incompatibility with the metallic sink materials [23,24]. The solution to this problem might be coating the material of the heat sink with nickel, molybdenum, or tungsten [25] or using nonmetallic materials as substrate material which might cause a significant change in thermal performance and increase the cost of production. A suitable fix for this kind of complication can be using non-metallic materials (like ceramic materials) in the heat sink which possess better heat transport capabilities.

Ceramic materials show excellent stability at very high temperatures and also negligible deformations at very harsh conditions [26–31]. And, few advanced ceramic materials possess excellent thermal properties that are suitable for their use in the mini/micro heat channel heat sinks. Vajdi et al. [32] studied the heat transfer and pressure drop in ZrB<sub>2</sub> heat sink with water as a working fluid. They found that the maximum temperature of the heat sink can be kept below 360 K by removing a heat flux of 3.6 MW/m<sup>2</sup>. Fattahi et al. [33] studied the performance of a heat exchanger made of AlN. Their results showed heat exchangers made of AlN can reach a heat transfer enhancement of 59% compared to that of Al<sub>2</sub>O<sub>3</sub> made one. The effectiveness of heat exchanger is also found to be improved by 26%. Vajdi et al. [34] on another study compared beryllium oxide (BeO) with alumina. They showed that the use of BeO led to ~100% heat transfer enhancement in comparison with alumina at a mass flow rate of 97.3 kg/h. Two other boron-based ceramic materials titanium diboride (TiB<sub>2</sub>) and hafnium diboride (HfB<sub>2</sub>) also possess excellent thermophysical properties [26–28,35,36]. Recently, the application of these ceramic materials is growing many interests in cooling technologies.

Though researchers have extensively studied the feasibility of the application of different ceramic materials in the mini/micro heat exchangers, there still exists no such comparison between the performance of these ceramic materials. The comparison could be crucial for the selection of the appropriate material to be used in the micro/mini channel heat sink. That would also offer the opportunity to use liquid metal cooling technology in several new fields. This study presents a 3-D numerical analysis of heat transfer in a rectangular mini channel heat sink with five different ceramic materials as substrate material. The thermal performance of the heat sink is compared by calculating the total thermal resistance with the 1-D thermal resistance model [3]. The temperature distribution of the heat sink with different substrate materials is also compared. The study also presents a comparison between the thermal and hydraulic performance of four different liquid metals (alloys of gallium) used as a coolant in the mini channel heat sink. After comparing the substrate materials and different coolants, the effect of different geometry parameters on the thermal and hydraulic performance of the heat sink is also tested. Finally, the application of these ceramic substrates with liquid metal coolants at very high-temperature is also discussed in the later sections.

## 2. Problem statement

A rectangular geometry of a mini channel heat sink was selected for the study having the dimensions ( $W \times L = 4\text{ cm} \times 4\text{ cm}$ ). The heat sink consists of 20 identical rectangular channels as shown in Fig. 1. The following geometry parameters were used in the comparison study between the substrate materials and different coolants: channel height

( $H = 5\text{ mm}$ ), channel width ( $W_c = 1\text{ mm}$ ), channel wall thickness ( $W_w = 1\text{ mm}$ ), thickness of the base ( $t_b = 2\text{ mm}$ ). The top surface of the heat sink was assumed to be having an adiabatic wall which generates a closed domain for fluid motion inside the mini channels. The study contains a numerical simulation of the fluid flow and heat transfer for a series of Reynolds numbers from 600 to 1800. Due to which laminar flow regimes could be assumed for all the cases. The analysis includes a comparison of five different substrate materials, four different liquid metals, and the effects of different geometry parameters on the overall performance of the heat sink. The properties of the substrate materials are shown in Fig. 2, Fig. 3, and Fig. 4. The properties of the working fluids are shown in Table 1.

The total pumping power needed for the fluid to transport through the heat sink is calculated by the following equation,

$$W_{pp} = n\Delta P A_{in} U_{in} \quad (1)$$

Where  $W_{pp}$  denotes the required pumping power,  $n$  denotes the number of rectangular channels,  $\Delta P$  denotes the pressure drop along a single channel,  $A_{in}$  and  $U_{in}$  are the area of the inlet and fluid velocity at inlet respectively.

The theoretical pressure drop is calculated from the following correlation [37],

$$\Delta P = f \frac{L}{D_h} \frac{\rho U_{in}^2}{2} \quad (2)$$

$$f_{app} Re = 21.04(x_{hyd})^{-0.434} \alpha^{-0.01} \quad \text{when } 0.001 < \alpha < 0.02 \quad (3)$$

$$f_{app} Re = 45.2(x_{hyd})^{-0.202} \alpha^{-0.094} \quad \text{when } 0.02 < \alpha < 0.1 \quad (4)$$

Where  $f_{app}$  is the friction factor,  $D_h$  is the hydraulic diameter,  $\alpha$  is the channel aspect ratio ( $\alpha = \frac{W_c}{H}$ ), and  $x_{hyd}$  is the hydrodynamic entrance region ( $x_{hyd} = \frac{L}{D_h Re}$ ).

The thermal performance of the heat sink is obtained by the 1D thermal resistance model [22]. According to the model, the total thermal resistance and maximum heat flux that can be extracted by the heat sink is calculated by the following equations,

$$R_{total} = \frac{\Delta T_{max}}{Q} \quad (5)$$

$$\Delta T_{max} = (T_{max,s} - T_{in}) \quad (6)$$

$$Q = q_b \times A_b \quad (7)$$

$$q_{max} = \frac{T_a - T_{in}}{R_{total} A_b} \quad (8)$$

Where,  $T_{max,s}$  and  $T_{in}$  are the maximum surface temperature of the heat source and fluid inlet temperature respectively. The term  $q_b$  denotes the heat flux applied at the base of the heat sink. The term  $A_b$  represents the surface area of the base of the heat sink.  $T_a$  is the maximum allowable temperature at the heat source. The term  $q_{max}$  is the maximum heat flux per unit area which can be removed by the heat sink at a fixed temperature rise ( $T_a - T_{in}$ ).

## 3. Mathematical formulation and numerical method

A 3-dimensional conjugate model is generated for the solution considering the following assumptions,

- Flow is steady-state, laminar, and incompressible.
- Radiative heat losses are neglected.
- Body forces are negligible.
- Constant fluid properties.
- Due to the identical geometry of all the rectangular channels, all the channels show identical heat and mass transfer properties. That's why a single channel can be selected for the analysis.

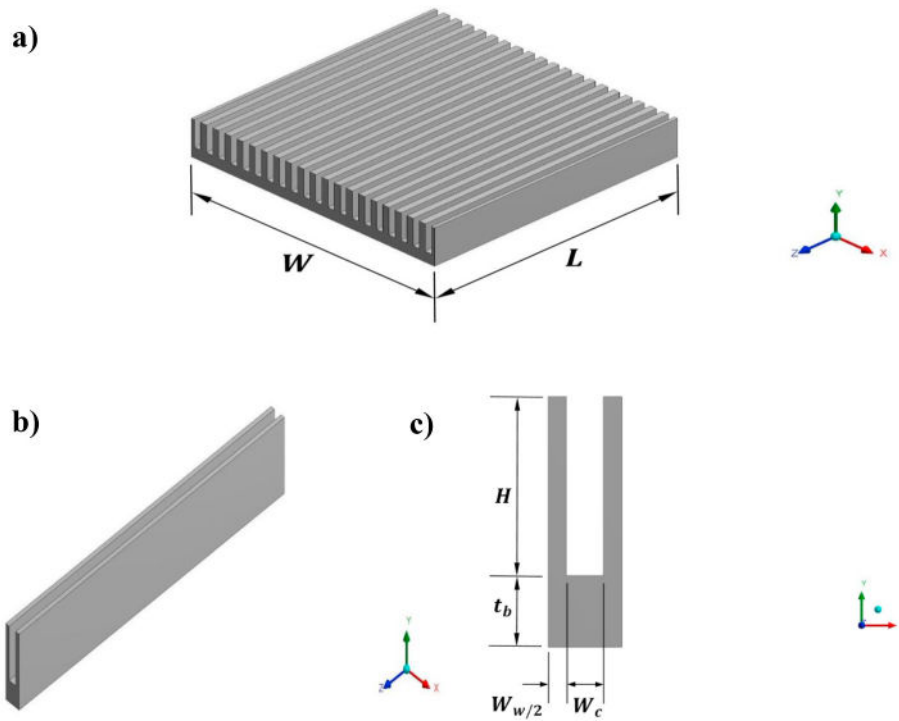


Fig. 1. a) 3D isometric view of the mini channel heat sink, b) 3D isometric view of a single channel, c) front view of the single-channel.

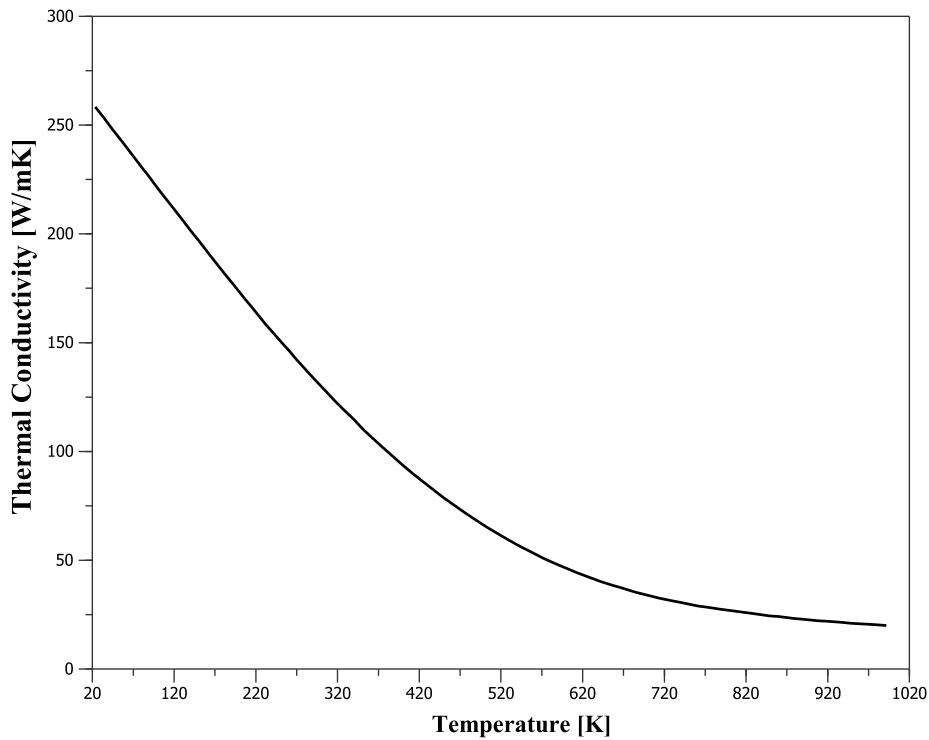


Fig. 2. Thermal conductivity of BeO [34].

By taking account of the mentioned assumptions, the following equations are obtained which regulate the fluid flow and heat transfer in the 3D channel,

In the fluid region,

- Conservation of mass

$$\nabla \cdot \nu = 0 \tag{9}$$

- Conservation of momentum

$$\rho(\nu \cdot \nabla \nu) = -\nabla p + \nabla \cdot (\mu \nabla \nu) \tag{10}$$

- Conservation of energy

$$\rho C_p(\nu \nabla T) = k \nabla^2 T \tag{11}$$

Where  $\nu$  denotes the velocity,  $p$  denotes the pressure,  $\mu$  denotes the dynamic viscosity,  $k$  denotes the thermal conductivity,  $C_p$  denotes the

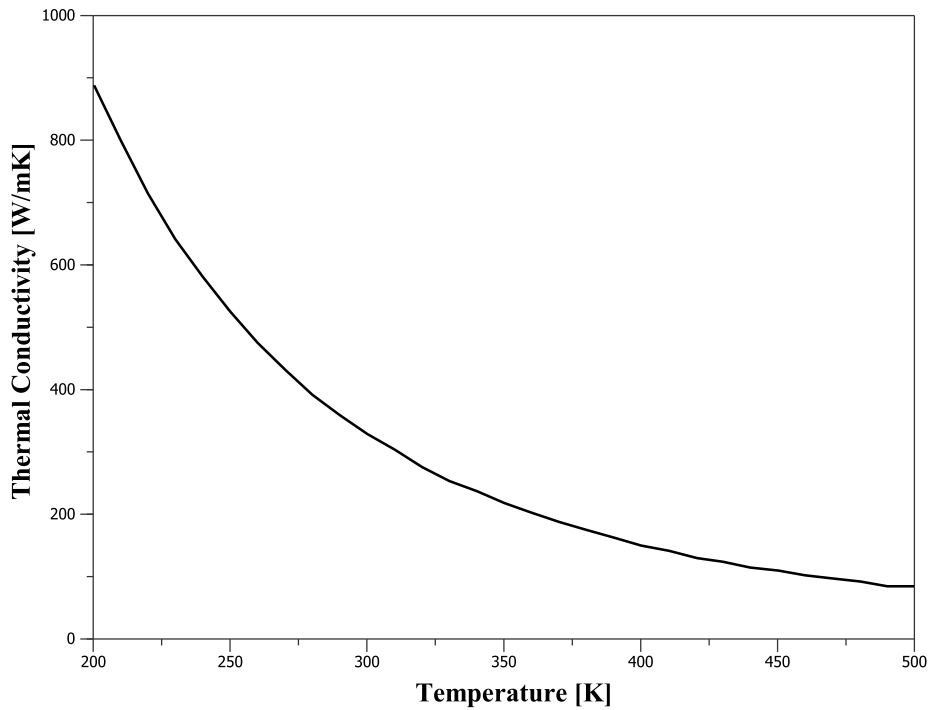


Fig. 3. Thermal conductivity of AlN [38].

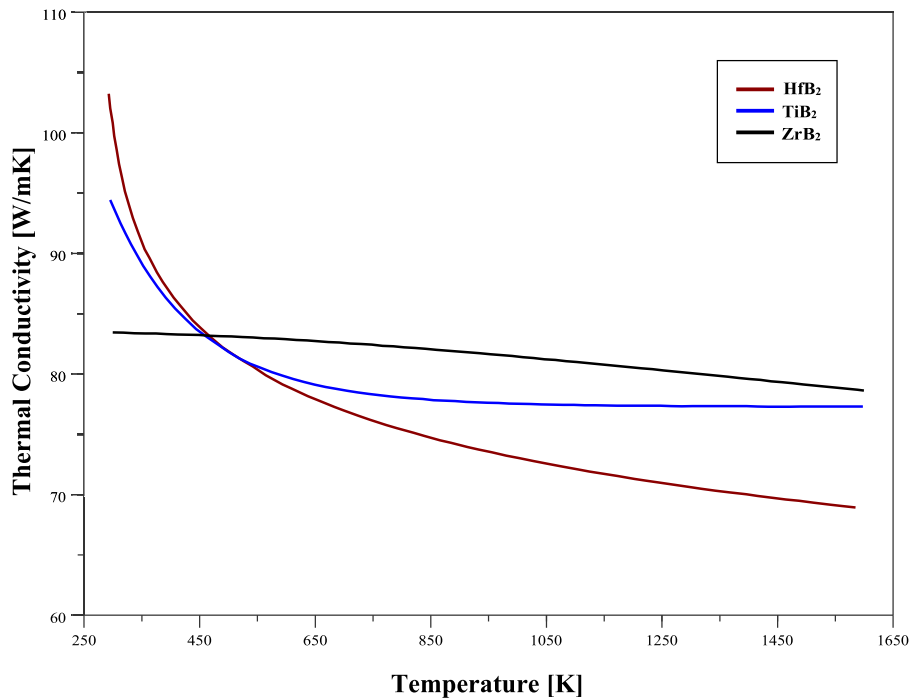


Fig. 4. Thermal conductivities of HfB<sub>2</sub>, TiB<sub>2</sub> and ZrB<sub>2</sub> [36].

specific heat capacity, and  $\rho$  denotes the density of the fluid.

For the solid region,

- Continuity equation

$$\nu = 0 \tag{12}$$

- Energy equation

$$k_s \nabla^2 T_s = 0 \tag{13}$$

Where  $k_s$  denotes the thermal conductivity and  $T_s$  denotes the temperature of the solid.

The boundary conditions for the model are summarized below:

For the solid domain, constant heat flux per unit area ( $q_b = 100 \text{ W/cm}^2$ ) was applied at the bottom wall ( $y = 0$ ). The symmetry boundary condition was applied at the left and right walls ( $x = 0, x = W_w + W_c$ ). The adiabatic wall boundary condition was applied at the top wall, the front and back wall of the sink ( $y = H + t_b, z = 0, z = L$ ). No-slip boundary conditions at the fluid-solid interface. For the fluid domain, uniform velocity ( $U_{in}$ ) with

**Table 1**  
Thermophysical properties of coolant materials [37].

Material	Density, $\rho$ $Kg/m^3$	Thermal conductivity, $k$ $(W/mK)$	Specific heat, $C_p$ $(J/KgK)$	Dynamic viscosity, $\mu$ $\times 10^{-3}$ $(Pa. s)$	Prandtl number
EGaInSn	6440	16.5	295	2.400	0.043
EGaIn	6280	26.6	404	1.990	0.030
GaSn	6300	30	365	2.192	0.027
GaIn	6363.2	39	365.4	2.210	0.021

constant temperature ( $T_{in}$ ) was applied at the inlet ( $z = 0$ ).

ANSYS FLUENT 17.0 was used for the numerical analysis. Pressure based 3D segregated solver was used which is based on the finite volume method. The computational domain was discretized with structured 3D hexahedral cells generated by the software ICEMCFD 17.0. The convective heat flux and the momentum equation was obtained by the second-order upwind scheme. The diffusive flux was computed with the second central differencing scheme. The classical SIMPLE algorithm was used for the pressure-velocity coupling. The under-relaxation factors used were for pressure = 0.3, momentum = 0.7 and energy = 1. Qualitative convergence had been judged by residual falling below  $10^{-6}$  for continuity and the velocity components and below  $10^{-10}$  for energy. The Quantitative convergence was judged by average heat source temperature and pressure at inlet remaining unchanged with subsequent iterations.

**4. Validation and mesh independence**

The numerical model was first validated against the simulation data mentioned in Yang et al. [22]. Secondly, a concise mesh independence test was done with five different grids generated by different sizes of hexahedral shaped elements. Fig. 5 represents the comparison between the present work and the numerical data obtained from Yang et al. [22]. The numerical model shows much competence with the literature work which proves its accuracy. The errors found at different channel heights (1 mm to 10 mm) on the total thermal resistance were 1.01%, 0.53%, 0.02%, 0.34%, and 0.12% respectively when compared with the data obtained from the literature. The errors associated with the required

**Table 2**  
Grid independence test for the model.

Number of elements	$R_{total}$ $(K/W)$	% difference	$W_{pp}$ $(W)$	% difference
654234	0.0179711	–	0.340710	–
796536	0.0179593	0.010	0.341885	0.344
926928	0.0179620	0.015	0.346552	1.347
1100000	0.0179627	0.004	0.350917	1.244
1338363	0.0179618	0.005	0.352395	0.420

pumping power when compared was found to be 8.18%, 4.93%, 2.11%, 1.14%, and 0.70% respectively at different channel heights. Since the errors associated with the required pumping power was comparatively more for the present numerical model, all the pumping power data for the present study are also compared with the theoretical correlations shown in later sections. From the comparisons, agreement between the numerical data with the theoretical correlations were found which will prove the accuracy of the numerical data further.

The grid independence test or mesh independence test is shown in Table 2. The entire domain (both solid and fluid domain) was discretized with structured hexahedral cells generated by the commercial software ICEMCFD 17.0. The grid independence test was done with aluminum nitride (AlN) as substrate material and Galinstan (EGaInSn) as coolant. The inlet velocity of the coolant was ( $U_{in} = 1m/s$ ). As seen from the grid independence test the deviation from an earlier grid at each level was less than 0.005% for the total thermal resistance and less than 0.5% for the pumping power when the generated grid contained more than 1.1 million elements. For further analysis, the grid generated having 1338363 elements was selected for the study.

**5. Results**

In this section, the effects of Reynolds number on the flow and thermal performance are evaluated for different substrate and coolant materials at first. The flow performance was compared by the required pumping power for fluid transport. The thermal performance was compared by the total thermal performance and maximum heat flux that can be extracted by the mini channel heat sink. The maximum heat flux that can be extracted by the heat sink was calculated by selecting

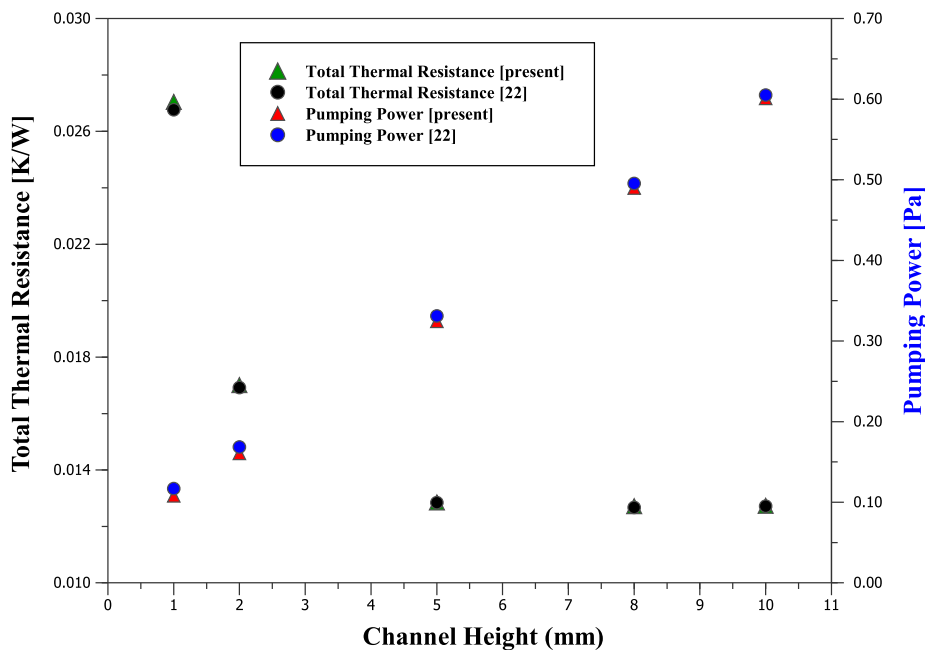


Fig. 5. Comparison between present work and literature [22], Ga<sub>68</sub>In<sub>20</sub>Sn<sub>12</sub> as a coolant and copper alloy as the heat sink material.

the maximum allowable temperature of the heat source to be ( $T_a = 350K$ ). In the later part, the effect of different geometry parameters of the mini channel on the overall performance of the heat sink is briefly explained. Lastly, several very high heat fluxes are applied on the heat sink with a fixed substrate and a liquid metal coolant, to predict the heat transfer characteristics of the heat sink at very high-temperature applications.

5.1. Comparison of the thermal and hydraulic performance of the working fluids

The comparison of the thermal and hydraulic performance of different working fluid is presented in this section. Aluminum nitride (AlN) was used as the substrate material for all the analyses.

First, the hydraulic performance of the coolants is compared by studying the required pumping power at different flow Reynolds number. Since the coolants used in this study were liquid metals. The coolants have a comparatively higher density comparing with other widely used coolants. The higher density of coolants is also responsible for them to face higher flow restrictions inside the channels. That explains the high pumping power requirements in the heat sink despite laminar flow regimes in the flow. The effect of flow Reynolds number on the required pumping power is shown in Fig. 6 for the working fluids. The required pumping power depends greatly on the inlet Reynolds number. The required pumping power is increased by about 59% upon increasing the flow Reynolds number from 600 to 900 for the coolant EGaInSn. Similar trends can be seen for the other working fluids as well. Though at  $Re = 600$ , the required pumping power is quite identical for all the coolants, at higher Reynolds number the variation in required pumping is quite significant among the four coolants. The least pumping power is needed for EGaIn due to its lower viscosity and density than the other materials. The pumping power requirements for GaIn and GaSn are nearly identical due to their similar dynamic viscosity and density. At lower flow Reynolds number, there is no significant effect of coolant selection on the required pumping power. But at higher Reynolds number, the selection of suitable coolant fluid is quite necessary. At  $Re = 1800$ , EGaInSn requires the largest pumping

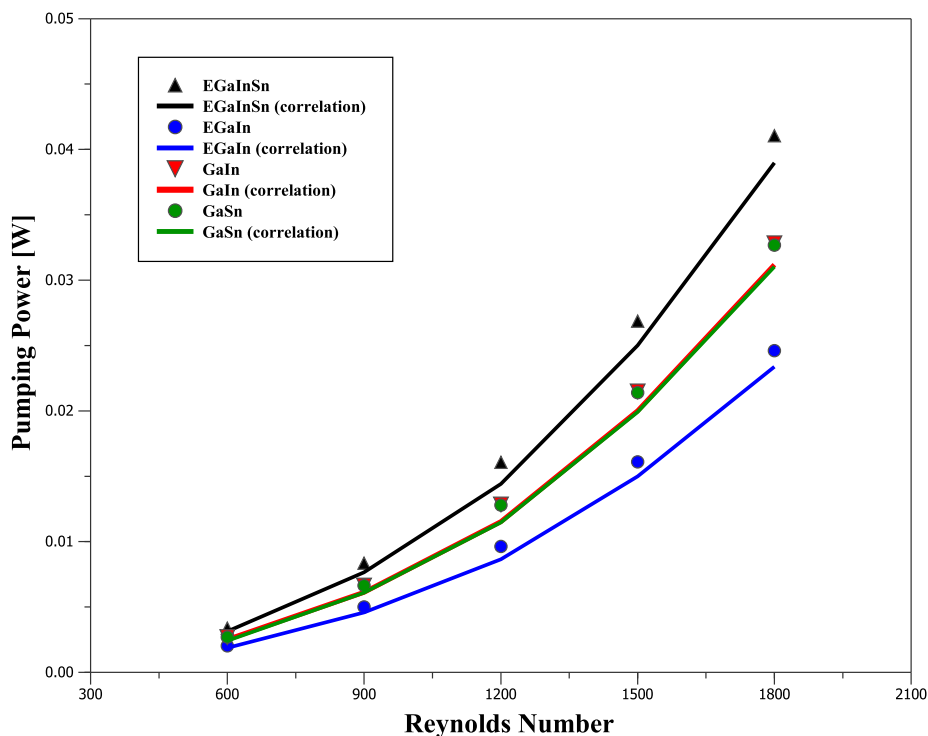


Fig. 6. Variation of pumping power with Reynolds number for different working fluids.

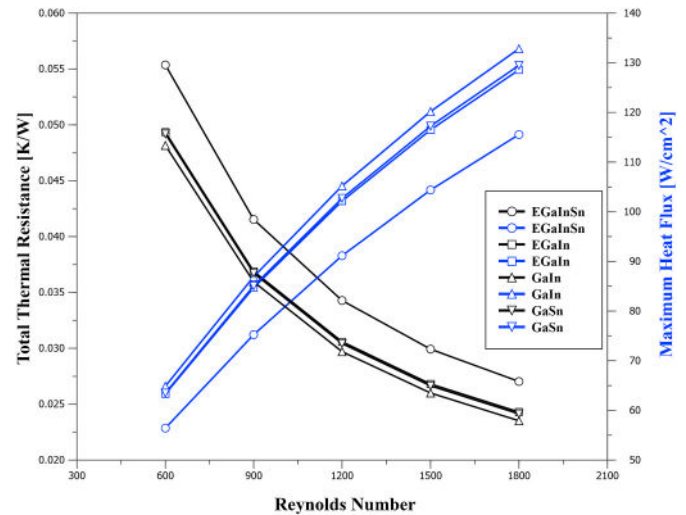


Fig. 7. Comparison of thermal performance of different coolants.

power since it has the highest density and dynamic viscosity. But, switching to GaIn can lower the pumping power requirements by 20%. If we switch to EGaIn, the pumping power requirements get reduced to about 40%.

The thermal performance of the coolants is compared by analyzing the total thermal resistance and maximum heat flux, as shown in Fig. 7. The effect of flow Reynolds number is also a vital thermal performance factor. The increase of Reynolds number from 600 to 900 allows us to increase the maximum heat flux value by about 33%. The total thermal resistance shows the opposite trend. That means, the increase in the flow Reynolds number reduces the total thermal resistance offered by the heat sink, while that allows increasing the maximum heat flux. The slope of the increase in the maximum heat flux decreases by the increase in the flow Reynolds number. At  $Re = 900, 1200, 1500,$  and  $1800$  the increase in the maximum heat flux is respectively about 33%, 21%, 14%, and 10% concerning the

maximum heat flux offered at lower Reynolds number. Now, we observe the total thermal resistance offered by different coolants in the heat sink. At all Reynolds number, maximum thermal resistance is offered by EGaInSn and the lowest total thermal resistance is offered by GaIn. GaSn and EGaIn shows quite identical performance due to their similar thermophysical properties. At  $Re = 1800$ , switching from GaInSn to GaIn can reduce the total thermal resistance about 13%. The maximum heat flux offered by the heat sink can be increased by about  $15\text{W}/\text{cm}^2$  by selecting GaIn instead of EGaInSn.

Finally, after evaluating the hydraulic and thermal performance of the coolants, it can be said that GaIn can offer the least thermal resistance and the maximum heat flux compared to all other coolants. EGaIn requires the least pumping power to run inside the mini channels.

### 5.2. Comparison of thermal performance of heat sink using different substrate materials

In this section, the thermal performance of the heat sink is presented with five different ceramic materials as a substrate material for the heat sink. GaIn was used as a coolant for all cases due to its better thermal performance found in the earlier section. Since the working fluid remains the same for all the analysis, the required pumping power and pressure drop are also the same for all the substrate materials.

Fig. 8 shows the total thermal resistance and maximum heat flux offered by the mini channel heat sink with five different substrate materials. The heat sink with aluminum nitride (AlN) shows the best performance since it has the highest thermal conductivity. The heat sink with AlN shows the lowest thermal resistance and the highest maximum heat flux. The maximum heat flux offered by the heat sink with BeO is next to AlN. TiB<sub>2</sub> and HfB<sub>2</sub> show quite identical performance due to having quite similar thermal conductivities in the temperature range of the heat sink. The heat sink having ZrB<sub>2</sub> offers the least maximum heat flux.

The temperature contours of the heat sink with five different ceramic materials are shown in Fig. 9. The contour plots suggest that heat sink with substrate material aluminum nitride shows much better temperature distribution because of its higher thermal conductivity than the other substrate materials. Better temperature distribution on the channel walls can reduce the possibility of excessive thermal stress

in any particular place. The contour plots in Fig. 9 also show the maximum temperature rise is towards the outlet of the channel.

### 5.3. Effect of geometric parameters on the overall thermal and hydraulic performance

In this section, the effects of different geometric parameters on the heat transfer capacity and required pumping power is briefly explained. The parameters selected for the present study were channel height, channel width, channel wall thickness, and thickness of the base. These parameters can greatly affect the thermal and hydraulic performance for a rectangular mini channel heat sink, which can be observed from the discussions presented in this section. For all the analysis, the substrate material and the coolant was aluminum nitride and GaIn respectively. The inlet velocity of the coolant was ( $U_{in} = 0.25\text{ m/s}$ ) for all the cases. A heat flux of  $100\text{ W}/\text{cm}^2$  was applied at the base.

The first parameter of interest is the channel height. The effect of channel height from  $2\text{mm}$  to  $7\text{mm}$  was studied by keeping the rest of the parameters fixed. The total thermal resistance and the required pumping power at different channel heights are shown in Fig. 10(a). When the channel height is increased by keeping the channel width fixed the solid-fluid interaction area is increased in the sidewalls of the channel, which increases the convective heat transfer rate. For this reason, the increase in the channel height causes a decrease in the total thermal resistance offered by the heat sink. However, at higher channel heights the conductive heat resistance starts to play a significant role in the total thermal resistance. For which reason the decrease in total thermal resistance is more at lower channel heights and comparatively less at higher channel heights. That can be seen by analyzing the slope of the graph of total thermal resistance which gets reduced by the increase in channel heights. The increase in channel height means more fluids need to be pushed through the channel at a constant velocity. Due to this, the increase in channel height is not always a feasible idea as an increase in channel height also requires a higher pumping power. That means while selecting the optimum channel height for the mini channel one should adjust between the thermal and hydraulic performance.

Next, the geometry parameter studied is the channel width. The channel width to be considered was between  $0.5\text{mm}$  to  $1.0\text{mm}$ . Fig. 10(b) shows the total thermal resistance and the required pumping power at different channel widths by keeping the other parameters

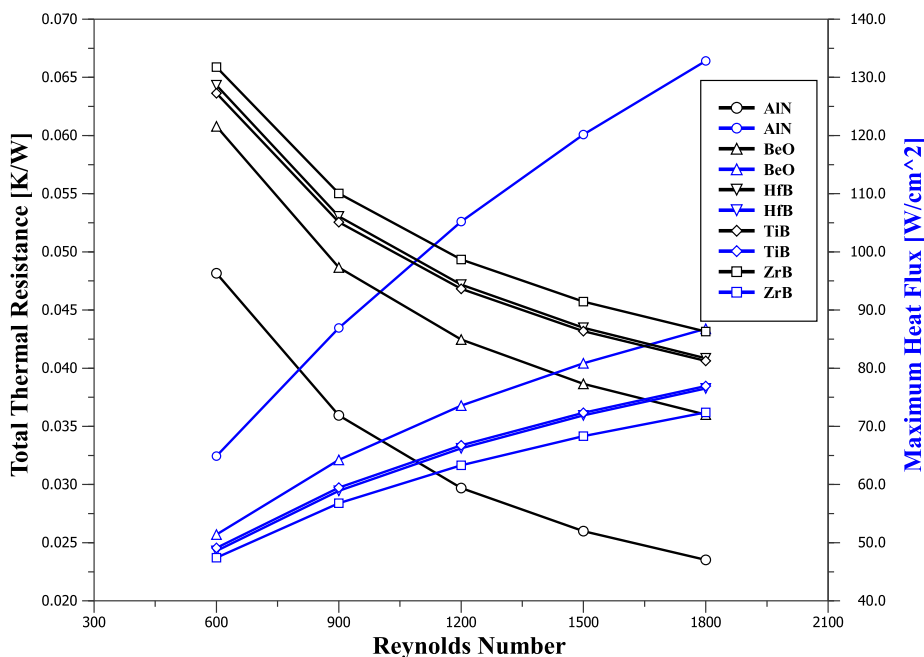


Fig. 8. Comparison of thermal performance of different substrate materials.

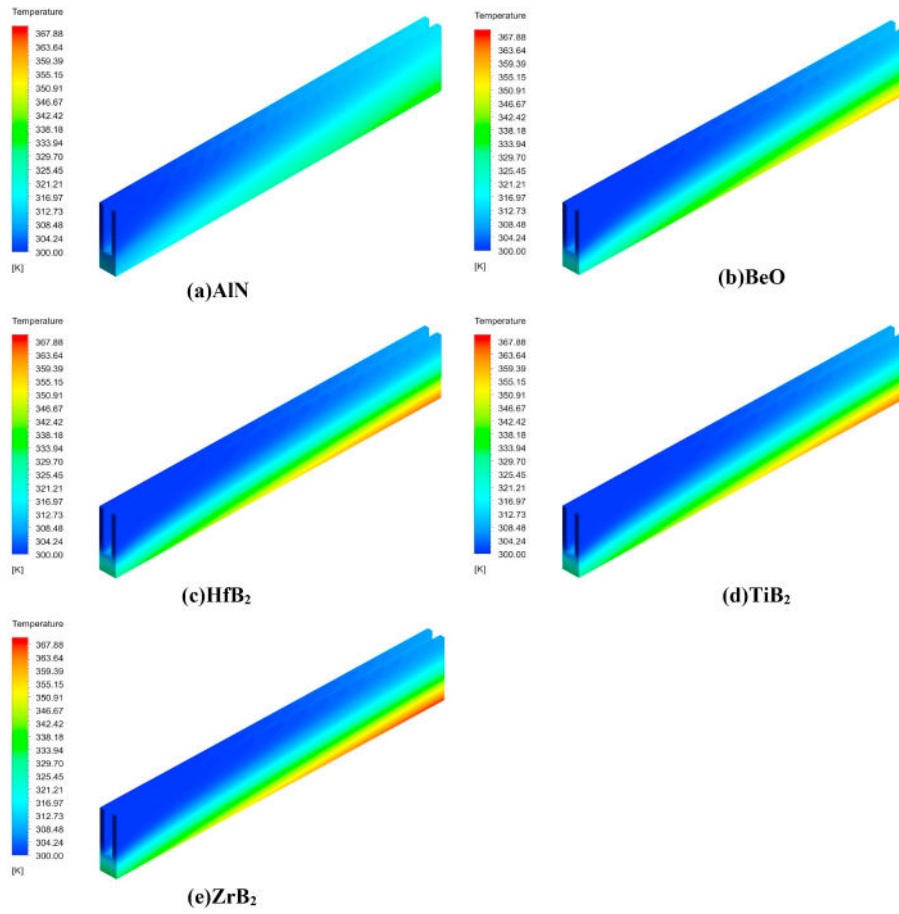


Fig. 9. Temperature contours with different substrate materials at  $Re = 1800$ .

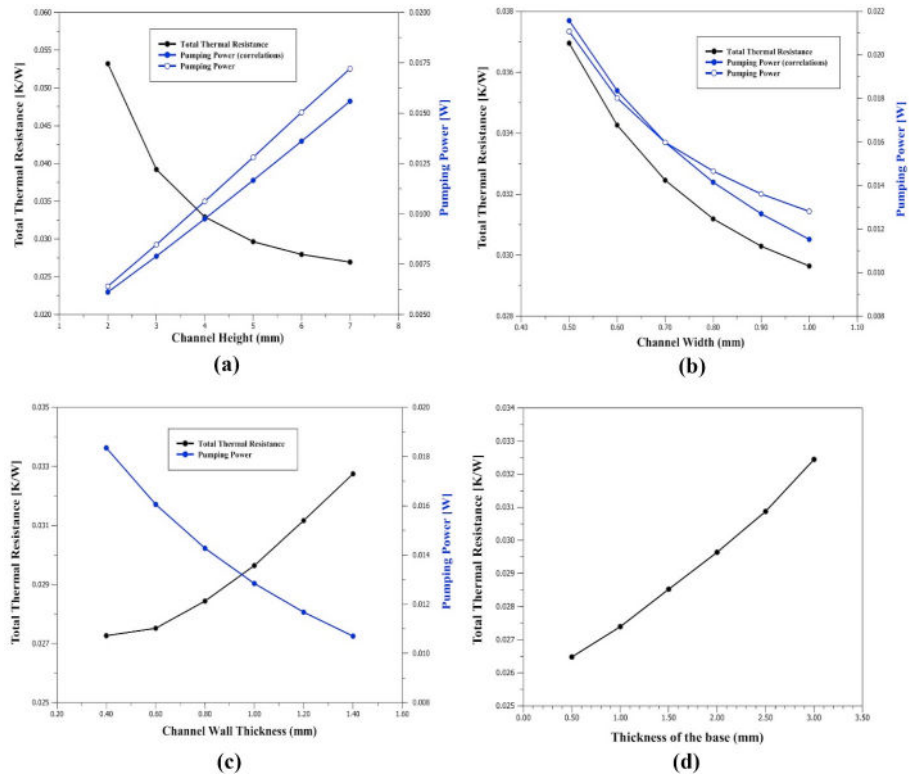


Fig. 10. Comparison of total thermal resistance and required pumping power at different geometry parameters: a) channel height, b) channel width, c) channel wall thickness, d) thickness of the base.

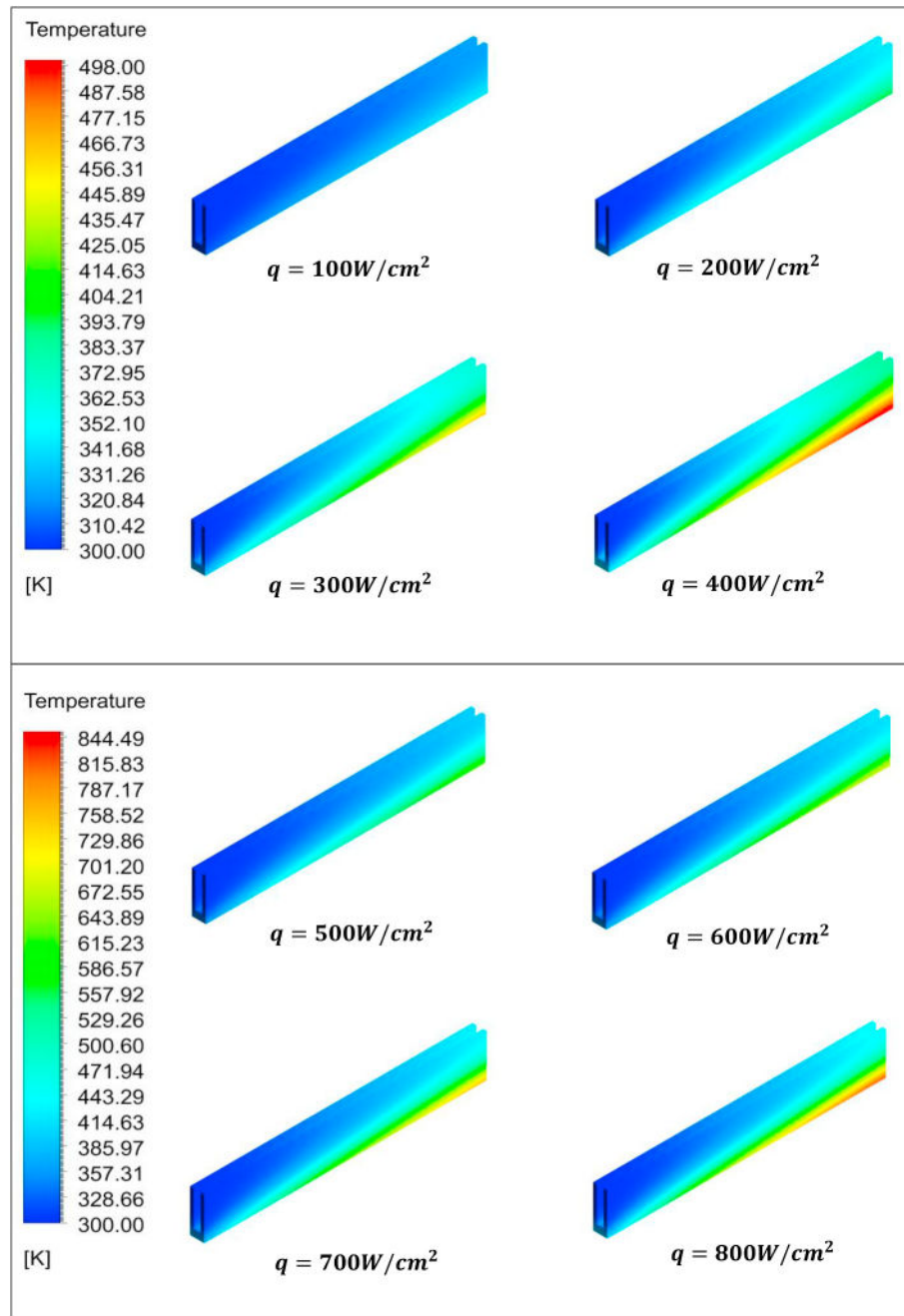


Fig. 11. Temperature contours with AIN substrate and GaIn coolant with different heat fluxes at  $Re = 1200$ .

fixed. The total thermal resistance diminishes as we increase the channel width. The decrease in total thermal resistance is due to the increased surface area for the solid-fluid interactions which causes the convective heat transfer rate to increase. The required pumping power also gets reduced as we can see from Fig. 10(b). The reason for requiring less pumping power is the lesser flow resistance faced by the liquid metal while flowing inside the mini channel. That also results in lower pressure drop inside the mini channel heat sink and the lesser pumping power requirements. There is another important factor to mention that, by keeping the width of the heat sink fixed at ( $W = 40\text{mm}$ ), when the width of the channel is adjusted with a fixed channel wall thickness, the number of channels inside the heat sink is also altered. The number of channels was calculated by the formula ( $n = W/(W_c + W_w)$ ). At lower channel widths, the number of channels is more. When the number of channels is more, the pressure drop faced

in each of the channels adds up and results in higher required pumping power. This is another reason for having a lower requirement of pumping power at higher channel widths. Following all these characteristics the width of the channels should be selected for a mini channel heat sink.

Fig. 10(c) shows the total thermal resistance and required pumping power at different channel wall thickness by keeping the other geometry parameters fixed. The channel wall contributes two different resistances in the total thermal resistance. One is the convective heat resistance from the side walls which remains constant for a fixed wall surface area and inlet velocity of the fluid. Another one is conductive heat resistance. The conductive heat resistance is more for a narrow wall. For a thicker wall, the conductive heat resistance is lesser. But this decrease in conductive heat resistance is not enough to reduce the total thermal resistance. Because the width of the heat sink is kept fixed at

( $W = 40\text{mm}$ ) in our analysis. When channel wall thickness is adjusted by keeping the channel width fixed, it increases or decreases the number of channels in the heat sink ( $n = W/(W_c + W_w)$ ). When the channel wall is thin, the number of channels is more which results in more fluid to enter the heat sink. That allows us to extract more heat from the heat sink, which decreases the total thermal resistance. For this reason, the increase in the channel wall thickness also increases the total thermal resistance of the heat sink as shown in Fig. 10(c). For the same reason, the required pumping power also changes by increasing or decreasing the thickness of the channel wall despite having the same channel geometry. Since the same geometry of the channel results in equal pressure drop across the channels, the pumping power is not compared with the correlations. It can be said that a thin channel wall offers a lower total thermal resistance but with high pumping power requirements. And a thick channel wall offers a higher total thermal resistance but with lower pumping power. For selecting the channel wall thickness, both of these factors must be kept in concentration.

The final parameter of interest is the thickness of the base plate of the heat sink. The total thermal resistance offered by the heat sink at the different thickness of the base is showed in Fig. 10(d). The base plate receives heat from its lower wall and part of the heat is transferred to the upper wall of the channel and transmitted to the fluid by convection. Another part of the heat is transmitted to the channel side-walls. A thin base plate will transmit more heat to the fluid and a thicker base plate will transmit more heat to the side walls. Therefore, a thinner base plate will hinder the transverse heat transport from the lower wall of the base to the channel wall. But the most important thing to consider is the conductive heat resistance, which is higher for a thick base plate. The effect of base thickness on the conductive heat resistance is generally significantly greater. For this reason, the total thermal resistance increases linearly with the thickness of the base plate. But while selecting the base plate thickness it should be considered that for high-temperature applications, a thin base plate will generate more thermal stress on the bottom part of the heat sink. The machining feasibility and the mechanical strength behavior should also be considered for selecting the thickness of the base of the heat sink.

#### 5.4. Application of the mini-channel heat sink at high-temperatures

One of the most important advantages of using a ceramic substrate in cooling technology is that it can be used in very high-temperature applications because it has good resistive properties against corrosion and high thermal stress. On the other hand, typically the usage of liquid metal cooling technology is used mostly at high-temperatures. Since aluminum nitride (AlN) and GaIn were found out to be the most efficient materials in the earlier sections, these are used as the materials in this section. Fig. 11 represents the temperature contours of a single rectangular channel with a range of heat flux applied at the bottom of the heat sink. The geometry parameters used for the study were channel height ( $H = 5\text{mm}$ ), channel width ( $W_c = 1\text{mm}$ ), channel wall thickness ( $W_w = 1\text{mm}$ ), and thickness of the base ( $t_b = 1\text{mm}$ ), and Reynolds number ( $Re = 1200$ ). For a clearer understanding of the temperature profile on the heat sink at high heat flux applications, the results are presented by two different temperature ranges. The first part shows result up to a temperature 500 K and the second part shows temperature contours up to 850 K.

The fluid's Reynolds number is limited to 1200 for all the analyses. The application of heat fluxes from  $100\text{ W/cm}^2$  to  $400\text{ W/cm}^2$  resulted in the maximum temperature of the heat sink to be limited to 500 K. The higher temperature region is towards the outlet near the applied heat flux. The maximum temperature of the heat sink is more than 800 K when the applied heat flux is  $800\text{ W/cm}^2$  as shown in Fig. 11. It

can be seen that temperature variation in the sink wall is lesser in applications involving lower heat fluxes. But there is a huge variation in temperature on the heat sink wall from the fluid inlet to the outlet at higher heat fluxes which could generate huge thermal stress. In such heavy heat flux applications, it is recommended that a high inlet flow velocity be used to get a reduced temperature variation.

## 6. Conclusions

The study presents a comparison of the thermal and hydraulic performance of four different gallium alloys, which are found to have excellent thermophysical properties to be used as a coolant in mini/microchannel heat sinks. The cooling performance of these working fluid is accompanied by five different ceramic materials as a substrate material in the heat sink. All the numerical data presented in this study are consistent with the theoretical correlations. The heat transfer capacity of the mini channel heat sink is analyzed by the 1-D thermal resistance model. By analyzing the results, the following concluding remarks are obtained:

- GaIn shows superior thermal performance than all other gallium alloys. By using GaIn as a working fluid compared to other coolants, the heat sink can obtain the lowest total thermal resistance.
- EGaIn requires the least pumping power amongst the working fluids.
- AlN shows better temperature distribution than other substrate materials on the heat sink.
- Heat sink with substrate material AlN has the lowest total thermal resistance followed by BeO.
- Heat sink with HfB<sub>2</sub> and TiB<sub>2</sub> show nearly identical thermal performance.
- Heat sink with substrate material ZrB<sub>2</sub> has the maximum thermal resistance out of the boron-based ceramic materials.
- The correlations presented for calculating the required pumping power show very good agreement with the numerical data.
- The geometry parameters of the rectangular channel can greatly influence the overall thermal and hydraulic performance of the heat sink.
- At high heat flux applications, there is a huge temperature variation on the heat sink wall.

Liquid metal cooling is an excellent new technology which, due to the higher heat transport capabilities of liquid metals, can be advantageous in many ways over other common cooling methods. Previously the use of this technology was limited to high-temperature applications in nuclear industries. Despite having excellent heat transport properties of liquid metals, their wide usage was always limited due to the limitations of the matching substrate materials. This present study by introducing newer compatible substrate materials offers a solution to the challenges of liquid metal cooling technology. Adding ceramic substrate can facilitate the use of this excellent liquid metal cooling technology without the possibility of corrosion and also save the extra cost of putting coatings on the substrate materials in mini/microchannel heat sink applications.

## Declaration of competing interest

The author declares that he has no known competing financial interests or personal relationships that could have appeared to influence the work reported in this paper.

## Appendix

$H$	channel height (m)	TiB <sub>2</sub>	titanium diboride
$L$	length of the heat sink ( $m$ )	BeO	beryllium oxide
$W$	width of the heat sink ( $m$ )	$A_b$	area of the base ( $m^2$ )
$W_w$	thickness of the channel wall ( $m$ )	$k$	thermal conductivity ( $W/mK$ )
$\Delta P$	pressure drop ( $Pa$ )	$x_{hyd}$	hydraulic entry length (m)
$W_c$	channel width ( $m$ )		
$D_h$	hydraulic diameter	Greek letters	
$t_b$	thickness of the base ( $m$ )	$\rho$	density ( $Kg/m^3$ )
$U_{in}$	velocity of the fluid at the inlet ( $m/s$ )	$\alpha$	channel aspect ratio
$T_{in}$	temperature of the fluid at inlet ( $K$ )	$\mu$	dynamic viscosity ( $Pa \cdot s$ )
$R_{total}$	total thermal resistance ( $K/W$ )		
$R_{cond}$	conductive heat transfer resistance ( $K/W$ )	Subscripts	
$R_{conv}$	convective heat transfer resistance ( $K/W$ )	in	inlet
$R_{cap}$	heat capacity thermal resistance ( $K/W$ )	out	outlet
$W_{pp}$	pumping power ( $W$ )	f	fluid
$Re$	Reynolds number	s	solid
$A_{in}$	area of inlet ( $m^2$ )	$f$	friction factor
$n$	number of channels	$hyd$	hydraulic
$q_{max}$	maximum heat flux per unit area ( $W/cm^2$ )	c	channel
MCHS	mini/micro channel heat sink	w	channel wall
AlN	aluminum nitride	$cond$	conduction
HfB <sub>2</sub>	hafnium diboride	$conv$	convection
ZrB <sub>2</sub>	zirconium diboride	$cap$	capacity

## References

- [1] D.B. Tuckerman, R.F.W. Pease, D.B. Tuckerman, R.F.W. Pease, High-performance heat sinking for VLSI, IEEE Electron. Device Lett. 2 (1981) 126–129, <https://doi.org/10.1109/EDL.1981.25367>.
- [2] S.J. Kim, Methods for thermal optimization of microchannel heat sinks, Heat Tran. Eng. 25 (2004) 37–49, <https://doi.org/10.1080/01457630490248359>.
- [3] D. Liu, S.V. Garimella, Analysis and optimization of the thermal performance of microchannel heat sinks, Int. J. Numer. Methods Heat Fluid Flow 15 (2005) 7–26, <https://doi.org/10.1108/09615530510571921>.
- [4] N.R. Kuppusamy, H.A. Mohammed, C.W. Lim, Numerical investigation of trapezoidal grooved microchannel heat sink using nanofluids, Thermochim. Acta 573 (2013) 39–56, <https://doi.org/10.1016/j.tca.2013.09.011>.
- [5] X.L. Xie, Z.J. Liu, Y.L. He, W.Q. Tao, Numerical study of laminar heat transfer and pressure drop characteristics in a water-cooled minichannel heat sink, Appl. Therm. Eng. 29 (2009) 64–74, <https://doi.org/10.1016/j.applthermaleng.2008.02.002>.
- [6] C. Min, C. Qi, E. Wang, L. Tian, Y. Qin, Numerical investigation of turbulent flow and heat transfer in a channel with novel longitudinal vortex generators, Int. J. Heat Mass Tran. 55 (2012) 7268–7277, <https://doi.org/10.1016/j.ijheatmasstransfer.2012.07.055>.
- [7] A. Datta, D. Sanyal, A.K. Das, Numerical investigation of heat transfer in micro-channel using inclined longitudinal vortex generator, Appl. Therm. Eng. 108 (2016) 1008–1019, <https://doi.org/10.1016/j.applthermaleng.2016.07.165>.
- [8] S. Chamoli, R. Lu, H. Chen, Y. Cheng, P. Yu, Numerical optimization of design parameters for a modified double-layer microchannel heat sink, Int. J. Heat Mass Tran. 138 (2019) 373–389, <https://doi.org/10.1016/j.ijheatmasstransfer.2019.04.032>.
- [9] J.F. Zhang, L. Jia, W.W. Yang, J. Taler, P. Oclon, Numerical analysis and parametric optimization on flow and heat transfer of a microchannel with longitudinal vortex generators, Int. J. Therm. Sci. 141 (2019) 211–221, <https://doi.org/10.1016/j.ijthermalsci.2019.03.036>.
- [10] X.D. Zhang, X.H. Yang, Y.X. Zhou, W. Rao, J.Y. Gao, Y.J. Ding, Q.Q. Shu, J. Liu, Experimental investigation of galinstan based minichannel cooling for high heat flux and large heat power thermal management, Energy Convers. Manag. 185 (2019) 248–258, <https://doi.org/10.1016/j.enconman.2019.02.010>.
- [11] W. Arshad, H.M. Ali, Experimental investigation of heat transfer and pressure drop in a straight minichannel heat sink using TiO<sub>2</sub> nanofluid, Int. J. Heat Mass Tran. 110 (2017) 248–256, <https://doi.org/10.1016/j.ijheatmasstransfer.2017.03.032>.
- [12] Y. Sui, P.S. Lee, C.J. Teo, An experimental study of flow friction and heat transfer in wavy microchannels with rectangular cross section, Int. J. Therm. Sci. 50 (2011) 2473–2482, <https://doi.org/10.1016/j.ijthermalsci.2011.06.017>.
- [13] C. Liu, J.T. Teng, J.C. Chu, Y.L. Chiu, S. Huang, S. Jin, T. Dang, R. Greif, H.H. Pan, Experimental investigations on liquid flow and heat transfer in rectangular micro-channel with longitudinal vortex generators, Int. J. Heat Mass Tran. 54 (2011) 3069–3080, <https://doi.org/10.1016/j.ijheatmasstransfer.2011.02.030>.
- [14] V.Y. Prokhorenko, V.V. Roshchupkin, M.A. Pokrasin, S.V. Prokhorenko, V.V. Kotov, Liquid gallium: potential uses as a heat-transfer agent, High Temp. 38 (2000) 954–968, <https://doi.org/10.1023/A:1004157827093>.
- [15] A. Miner, U. Ghoshal, Cooling of high-power-density microdevices using liquid metal coolants, Appl. Phys. Lett. 85 (2004) 506–508, <https://doi.org/10.1063/1.1772862>.
- [16] R. Zhang, M. Hodes, N. Lower, R. Wilcoxon, Thermo-fluid characteristics of a minichannel heat sink cooled with liquid metal, Annu. IEEE Semicond. Therm. Meas. Manag. Symp. (2013) 159–165, <https://doi.org/10.1109/SEMI-THERM.2013.6526822>.
- [17] A. Miner, U. Ghoshal, Cooling of high-power-density microdevices using liquid metal coolants, Appl. Phys. Lett. 85 (2004) 506–508, <https://doi.org/10.1063/1.1772862>.
- [18] G. Bo, L. Ren, X. Xu, Y. Du, S. Dou, Recent progress on liquid metals and their applications, Adv. Phys. X. 3 (2018) 1446359, <https://doi.org/10.1080/23746149.2018.1446359>.
- [19] D.S. Evans, A. Prince, Thermal analysis of Ga–In–Sn system, Met. Sci. 12 (1978) 411–414, <https://doi.org/10.1179/030634578790434025>.
- [20] Y.G. Deng, J. Liu, Y.X. Zhou, Liquid metal based mini/micro channel cooling device, Proc. 7th Int. Conf. Nanochannels, Microchannels, Minichannels 2009, ICNMM2009, American Society of Mechanical Engineers Digital Collection, 2009, pp. 253–259, <https://doi.org/10.1115/ICNMM2009-82046>.
- [21] X. Xiang, J. Yang, A. Fan, W. Liu, A comparison between cooling performances of water-based and gallium-based micro-channel heat sinks with the same dimensions, Appl. Therm. Eng. 137 (2018) 1–10, <https://doi.org/10.1016/j.applthermaleng.2018.03.063>.
- [22] X. Yang, S. Tan, Y. Ding, J. Liu, Flow and thermal modeling and optimization of micro/mini-channel heat sink, Appl. Therm. Eng. 117 (2017) 289–296, <https://doi.org/10.1016/j.applthermaleng.2016.12.089>.
- [23] Y.G. Deng, J. Liu, Corrosion development between liquid gallium and four typical metal substrates used in chip cooling device, Appl. Phys. Mater. Sci. Process 95 (2009) 907–915, <https://doi.org/10.1007/s00339-009-5098-1>.
- [24] F. Barbier, J. Blanc, Corrosion of martensitic and austenitic steels in liquid gallium, J. Mater. Res. 14 (1999) 737–744, <https://doi.org/10.1557/JMR.1999.0099>.
- [25] M. Tawk, Y. Avenas, A. Kedous-Lebouc, M. Petit, Numerical and experimental investigations of the thermal management of power electronics with liquid metal mini-channel coolers, IEEE Trans. Ind. Appl. 49 (2013) 1421–1429, <https://doi.org/10.1109/TIA.2013.2252132>.
- [26] S. Nekahi, M. Vajdi, F. Sadegh Moghanlou, K. Vaferi, A. Motallebzadeh, M. Özen, U. Aydemir, J. Sha, M. Shahedi Asl, TiB<sub>2</sub>–SiC-based ceramics as alternative efficient micro heat exchangers, Ceram. Int. 45 (2019) 19060–19067, <https://doi.org/10.1016/j.ceramint.2019.06.150>.
- [27] M. Vajdi, F. Sadegh Moghanlou, Z. Ahmadi, A. Motallebzadeh, M. Shahedi Asl, Thermal diffusivity and microstructure of spark plasma sintered TiB<sub>2</sub> [sbn] SiC[sbn]Ti composite, Ceram. Int. 45 (2019) 8333–8344, <https://doi.org/10.1016/j.ceramint.2019.01.141>.
- [28] E. Wuchina, M. Opeka, S. Causey, K. Buesking, J. Spain, A. Cull, J. Routbort, F. Gutierrez-Mora, Designing for ultrahigh-temperature applications: the mechanical and thermal properties of HfB<sub>2</sub>, HfCx, HfNx and  $\alpha$ Hf(N), J. Mater. Sci., Springer, 2004, pp. 5939–5949, <https://doi.org/10.1023/B:JMSSC.0000041690.06117.34>.
- [29] M. Shahedi Asl, Y. Azizian-Kalandaragh, Z. Ahmadi, A. Sabahi Namini, A. Motallebzadeh, Spark plasma sintering of ZrB<sub>2</sub>-based composites co-reinforced with SiC whiskers and pulverized carbon fibers, Int. J. Refract. Metals Hard Mater. 83 (2019) 104989, <https://doi.org/10.1016/j.jrmhm.2019.104989>.
- [30] L. Zhang, D.A. Pejaković, J. Marschall, M. Gasch, Thermal and electrical transport properties of spark plasma-sintered HfB<sub>2</sub> and ZrB<sub>2</sub> ceramics, J. Am. Ceram. Soc. 94 (2011) 2562–2570, <https://doi.org/10.1111/j.1551-2916.2011.04411.x>.
- [31] F. Sadegh, M. Vajdi, A. Motallebzadeh, J. Sha, Numerical analyses of heat transfer

- and thermal stress in a ZrB<sub>2</sub> gas turbine stator blade, *Ceram. Int.* 45 (2019) 17742–17750, <https://doi.org/10.1016/j.ceramint.2019.05.344>.
- [32] M. Vajdi, F. Sadegh Moghanlou, E. Ranjbarpour Niari, M. Shahedi Asl, M. Shokouhimehr, Heat transfer and pressure drop in a ZrB<sub>2</sub> microchannel heat sink: a numerical approach, *Ceram. Int.* 46 (2020) 1730–1735, <https://doi.org/10.1016/j.ceramint.2019.09.146>.
- [33] M. Fattahi, K. Vaferi, M. Vajdi, F. Sadegh Moghanlou, A. Sabahi Namini, M. Shahedi Asl, Aluminum nitride as an alternative ceramic for fabrication of microchannel heat exchangers: a numerical study, *Ceram. Int.* (2020), <https://doi.org/10.1016/j.ceramint.2020.01.195> 0–1.
- [34] M. Vajdi, M. Shahedi Asl, S. Nekahi, F. Sadegh Moghanlou, S. Jafarholnejad, M. Mohammadi, Numerical assessment of beryllium oxide as an alternative material for micro heat exchangers, *Ceram. Int.* 46 (2020) 19248–19255, <https://doi.org/10.1016/j.ceramint.2020.04.263>.
- [35] M. Mallik, A.J. Kailath, K.K. Ray, R. Mitra, Electrical and thermophysical properties of ZrB<sub>2</sub> and HfB<sub>2</sub> based composites, *J. Eur. Ceram. Soc.* 32 (2012) 2545–2555, <https://doi.org/10.1016/j.jeurceramsoc.2012.02.013>.
- [36] S. Nekahi, K. Vaferi, M. Vajdi, F. Sadegh Moghanlou, M. Shahedi Asl, M. Shokouhimehr, A numerical approach to the heat transfer and thermal stress in a gas turbine stator blade made of HfB<sub>2</sub>, *Ceram. Int.* 45 (2019) 24060–24069, <https://doi.org/10.1016/j.ceramint.2019.08.112>.
- [37] A. Muhammad, D. Selvakumar, A. Iranzo, Q. Sultan, J. Wu, Comparison of pressure drop and heat transfer performance for liquid metal cooled mini-channel with different coolants and heat sink materials, *J. Therm. Anal. Calorim.* (2020), <https://doi.org/10.1007/s10973-020-09318-2>.
- [38] G.H.B.K. Sahoo, Pyroelectric property of binary nitrides (AlN, GaN and InN), *Int. J. Thermophys.* 123 (2019) 1–10, <https://doi.org/10.1007/s10765-019-2481-9>.